Exosome-based biomimetic nanoparticles targeted to inflamed joints for enhanced treatment of rheumatoid arthritis

Feili Yan
Southwest Medical University
Zhirong Zhong
Southwest Medical University
Yao Wang
Southwest Medical University
Hui Li
Southwest Medical University
Zhiqiang Mei
Southwest Medical University
Yue Feng
Southwest Medical University
Xiang Chen
Southwest Medical University
liang Cai
Southwest Medical University
Chunhong Li (lispringhong@126.com)
Southwest Medical University

Research

Keywords: Dexamethasone sodium phosphate, Biomimetic, Exosomes, Folic acid, Rheumatoid arthritis

Posted Date: June 9th, 2020

DOI: https://doi.org/10.21203/rs.3.rs-33553/v1

Version of Record: A version of this preprint was published on August 20th, 2020. See the published version at https://doi.org/10.1186/s12951-020-00675-6.

Abstract

Backgroud:

Glucocorticoids (GCs) show powerful treatment effect on rheumatoid arthritis (RA). However, the clinical application is limited by their nonspecific distribution after systemic administration and serious adverse reactions during long-term administration. To achieve better treatment and reduce side effect, we here established a biomimetic exosome (Exo) encapsulating dexamethasone sodium phosphate (Dex) nanoparticle (Exo/Dex), whose surface was modified with folic acid (FA)-polyethylene glycol (PEG)-cholesterol (Chol) compound to attain FPC-Exo/Dex active targeting drug delivery system.

Results

The size of FPC-Exo/Dex was 128.43 ± 16.27 nm, with a polydispersity index (PDI) of 0.36 ± 0.05, and the Zeta potential was − 22.73 ± 0.91 mV. The encapsulation efficiency (EE) of the preparation was 10.26 ± 0.73%, with drug loading efficiency (DLE) of 18.81 ± 2.05%. *In vitro* study showed this system displayed enhanced endocytosis and excellent anti-inflammation effect against RAW264.7 cells by suppressing pro-inflammatory cytokines and increasing anti-inflammatory cytokine. Further biodistribution study showed the fluorescence intensity of FPC-Exo/Dex was stronger than other Dex formulations in joints, suggesting its enhanced accumulation to inflammation sites. *In vivo* pharmacodynamic experiment displayed FPC-Exo/Dex could preserve the bone and cartilage of CIA mice better and significantly reduce inflamed joints. Next *in vivo* safety evaluation demonstrated this biomimetic drug delivery system had no obvious hepatotoxicity and exhibited desirable biocompatibility.

Conclusion

The present study provides a promising strategy for using exosome as nanocarrier to enhance the therapeutic effect of GCs against RA.

1. Introduction

Rheumatoid arthritis (RA) is a chronic autoimmune disease whose pathophysiology is unclear [1]. As it progresses, articular cartilage and bone were destroyed, which can cause disability eventually [2, 3]. This progression may be driven by pro-inflammatory cytokines such as tumor necrosis factor (TNF)-α and the interleukins (IL)-1β and IL-6, as well as the inflammatory mediators inducible nitric oxide synthase and epoxidase [4, 5]. Glucocorticoids (GCs), one of the most widely used first-line drugs against RA, can control inflammation and relieve pain quickly by inhibiting the secretion of pro-inflammatory cytokines and up-regulating anti-inflammatory protein IL-10 [6, 7], which further inhibits the secretion of pro-inflammatory cytokines. However, long-term use of systemic, high-dose glucocorticoids is associated with serious adverse effects, such as decreased immunity, hyperglycemia and osteoporosis [8].

Delivering anti-RA drugs within nanoparticles may help target the drugs to inflamed tissues, thereby improving therapeutic efficacy and reducing adverse effects [8, 9]. Nanoparticles can accumulate at inflammatory sites through a process known as “extravasation through leaky vasculature and subsequent inflammatory cell-mediated sequestration” (ELVIS), which is analogous to the “enhanced permeability and retention” (EPR) effect that can lead nanoparticles to accumulate in solid tumors.

Indeed, targeted delivery of glucocorticoids against RA has already been achieved using liposomes, physically encapsulated micelles and polymer nanoparticles [2, 10–12]. However, liposomes are poor at evading host immune system clearance, they are unstable and they persist in circulation for only short periods [13, 14]. Physically encapsulated micelles are unstable in circulation because they are diluted and they can interact with proteins and other components of plasma [2, 3]. Polymer nanoparticles may be more stable than liposomes and physically encapsulated micelles, but their long-term biocompatibility and safety pose challenges [2, 5]. Consequently, developing more reliable and powerful nanocarriers is highly desired.

Exosomes have emerged as an alternative to those exogenous nanoparticles [15, 16]. These membrane-enclosed vesicles with sizes of 40–150 nm are naturally secreted by various cell types, which endow them with fascinating natural properties such as low cytotoxicity, non-immunogenicity, desirable biocompatibility, specific targeting capacity and prolonged systemic circulating ability [15, 17–19]. These superior properties making them ideal drug delivery nanocarriers. Moreover, exosome-based nanoparticles drug delivery has been successfully applied in loading various drugs for different diseases treatment, such as cancer, Parkinson, renal and brain inflammation, but have been rarely used in RA so far [19–22]. However, the exosome-based drug delivery existed flaw in selective accumulation to target sites *in vivo* [21–23].

Study on the pathological microenvironment of RA suggested that inflamed areas contain abundant activated macrophages that express folic acid receptors (FRs) on their surface, particularly FRβ [24, 25]. So, we reasoned that it may be effective to construct exosome-based nanoparticles coating with folic acid (FA) for enhancing accumulating ability by active targeting effect to FRβ *in vivo*. Therefore, we used exosomes to encapsulate dexamethasone sodium phosphate (Dex), one of the most frequently used GCs to treat RA in clinical, to obtain Exo/Dex nanoparticle firstly. Then, we modified it with FA-polyethylene glycol (PEG)-cholesterol (Chol) compound to prepare FPC-Exo/Dex active targeting drug delivery. Meanwhile liposome drug delivery system (Lip/Dex) was fabricated for comparative study to Exo/Dex in this research. Properties of these nanoparticles were characterized *in vitro*. Then the internalization and anti-inflammatory effects to lipopolysaccharide-activated RAW264.7 cells were examined. Furthermore their biodistribution, therapeutic efficacy against RA and *in vivo* safety were studied in mice with collagen-induced arthritis (CIA).

2. Material And Methods

2.1 Materials

Dexamethasone sodium phosphate was supplied by Solarbio Science & Technology (Beijing, China). Methanol and acetonitrile (HPLC grade) were purchased from Kelong Chemical Reagent Factory (Chengdu, China). Rabbit monoclonal antibodies against CD63 or CD9 as well as horseradish peroxidase-conjugated goat anti-rabbit IgG were purchased from Abcam (UK). SDS-PAGE kits and polyvinylidene fluoride membranes were obtained from Sigma (USA). Complete and incomplete Freund's adjuvant and bovine type II collagen were acquired from Chondrex (USA). ELISA kits were from Thermo Fisher (Austria). Fluorescent dyes PKH26 and PKH67 kits were purchased from Beijing Baiao Laibo Technology; 1, 1'-Dioctadecyl-3, 3, 3', 3'-tetramethylindodicarbocyanine perchlorate (DID), 3-(4,5-dimethylthiazol-2-yl)-2,5-diphenyltetrazolium bromide (MTT), FITC-labeled phalloidin DAPI and Lipopolysaccharide (LPS) were supplied by Beijing Solarbio Science & Technology. Other reagents were analytical grade.

2.2 Cells and animals

RAW 264.7 murine macrophages and human umbilical vein endothelial cells (HUVEC) (Chinese Academy of Sciences, Shanghai, China) were cultured in DMEM/HIGH GLUCOSE medium (Hyclone, USA) with 10% fetal bovine serum(FBS) (Gibco, USA) and 1% (v/v) penicillin/streptomycin (Hyclone, USA).

Male DBA/1 mice (8 weeks old) were purchased from Charles River (Beijing, China). All animal experiments were in accordance with The Animal Ethics Committee of Southwest Medical University.

2.3 Isolation and characterization of exosomes

When RAW 264.7 cultures reached the logarithmic phase of growth, cells were switched to FBS-free medium for 24 h, after which the medium was collected and replaced with fresh FBS-free medium. The cultures were incubated for another 24 h, then the medium was collected again. The two volumes of collected medium were pooled, exosomes were isolated using a gradient centrifugation protocol [20] with some modification. Firstly, the medium was centrifuged at 2000 *g* for 10 min and then at 10,000 *g* for 30 min to remove cellular debris. Next, the supernatant was concentrated to about 30% of the original volume at 2,000 *g* for 8 min using ultrafiltration tube (MWCO = 10,000). Finally, the supernatant was centrifuged at 120,000 *g* for 70 min in an ultracentrifuge (QPTimaMAX-XP Ultra-High, Beckman Coulter, USA). The pellets were washed with large volume cold phosphate-buffered saline (PBS) and centrifuged at 120,000 *g* for 70 min again to ensure maximal exosome purity. All centrifugation procedures were performed at 4 °C. The pellet was re-suspended in PBS and stored at -80 °C. The amount of exosomes was estimated using a Bradford assay (Bio-Rad Laboratories, Shanghai, China).

Size, polydispersity index (PDI) and zeta potential of purified exosomes were determined using dynamic light scattering (Malvern Zetasizer Nano ZS90, Malvern Instruments, UK). Their morphology was examined using transmission electron microscopy (HT7700, Hitachi, Japan). The presence of CD63 and CD9 on the exosome surface were measured by western blotting. These proteins serve as markers of exosomes derived from mammalian cells [18, 26].

2.4 Preparation of Exo/Dex and FPC-Exo/Dex

To load Dex into exosomes, exosomes (100 μg) were mixed with Dex (300 μg) in PBS with the concentration of trehalose was 80 nM, trehalose was added to avoid the aggregation of exosomes during electroporation. The mixture was subjected to electroporation at room temperature using a double poring pulse (200 V, 5 ms) and transfer pulse of five pulses (20 V, 50 ms) in a 1-cm electroporation cuvette and a NEPA21 Type II electroporater (NEPA genes, Tokyo, Japan). Then un-encapsulated Dex was removed by ultracentrifugation (100,000 *g*, 60 min, 4 °C). The Dex-loaded exosomes (Exo/Dex) were resuspended in PBS and incubated in 37 °C for 1 h to restore the membrane.

The FA-PEG-Chol conjugate was prepared as described in Supplementary Materials. The Chol end of FA-PEG-Chol was inserted into the lipid bilayer membrane of Exo/Dex by post-insertion [22]. Exo/Dex and FA-PEG-Chol ligands were mixed in a mass ratio of 1:5 and incubated at 37 °C for 2 h. Free ligands were removed by centrifugation at 3000 *g* for 10 min, giving rise to FPC-Exo/Dex. The amount of FA incorporated was determined by comparison of the UV_{285} value to a standard curve of folic [27, 28].

2.5 Preparation of Dex-loaded anion liposomes (Lip/Dex) as control group

Dex-loaded anionic liposomes were prepared in order to compare with exosome-based drug delivery systems. Anionic liposomes were prepared using ethanol injection as described [29]. Firstly, 40 mg of yolk lecithin, 10 mg of cholesterol and 10 mg of Dex were dissolved in 3 mL ethanol, and the solution was slowly injected into 5 mL PBS (pH 7.4) while stirring. The solution was slowly stirred under bath conditions at 40 °C for 2 h, and the solution was filtered through 0.45-μm and 0.22-μm membrane successively, yielding Lip/Dex.

2.6 Characterization of different Dex preparations

Size, PDI and zeta potential of all preparations were determined using dynamic light scattering, and morphology of FPC-Exo/Dex were examined by transmission electron microscopy. Encapsulation efficiency (EE) and drug loading efficiency (DLE) were measured using high-performance liquid chromatography (HPLC). Briefly, each formulation was divided into two equal portions, one of which was demulsified with 10% methanol, and the amount of total drug (W_t) was measured by HPLC. The free drug in the second portion (W_e) was pelleted by ultracentrifugation and weighed. EE was calculated using the equation $EE = W_e / W_t \times 100\%$. EE of Lip/Dex was determined in the same way.

The amount of exosomes (W_s) was estimated by BCA assay to calculate DLE according to the equation $DLE = W_e / (W_t + W_s) \times 100\%$. An equal amount of Lip/Dex was dried and weighed (W_p) to calculate DLE according to the equation $DLE = W_e / W_p \times 100\%$.

2.7 *In vitro* cumulative drug release study

FPC-Exo/Dex, Exo/Dex, Lip/Dex, or free Dex (40 μg of Dex contained in all preparations) were added to 1 mL PBS (pH 7.4) in a dialysis bag with a molecular weight cut-off of 3000 Da. The bag was placed in 30 mL PBS and shaken at 37 °C at 1000 rpm. At predetermined time points, 200 μL of release medium

was collected and immediately replaced with an equal volume of fresh medium. Dex concentration was determined by HPLC, and the cumulative amount released was calculated.

2.8. Toxicity assay of nanoparticles by MTT

RAW264.7 cells and HUVEC in logarithmic growth phase were digested into single-cell suspensions and seeded in 96-well plates at 1×10^4 cells per well, then incubated at 37 °C overnight. FPC-Exo/Dex, Exo/Dex and Dex were prepared in culture medium without serum or antibiotics, and 200 μL of each preparation was added to wells at Dex concentrations of 5–25 μg/mL. After 24 h, the medium was discarded, and 20 μL of MTT (5 mg/mL) solution and 180 μL of complete medium were added. Cells were cultured for another 4 h, then medium was replaced with 150 μL DMSO and cultures were shaken for 15 min at 37 °C. Absorbance at 490 nm was measured using a Varioskan Flash microplate reader (Thermo Fisher, USA). Relative cell viability was calculated using the equation: Cell viability = (sample − blank) / (negative control − blank) × 100%.

2.9 Cellular uptake study by flow cytometry and confocal laser scanning microscopy

Lip/Dex, Exo/Dex and FPC-Exo/Dex were labeled with PKH67 or PKH26 according to the dye manufacturer's protocol. PKH67-labeled Dex formulations were incubated for 2 h with resting or lipopolysaccharide (LPS)-activated (stimulated for 24 h with LPS at a final concentration of 100 ng/mL) RAW264.7 cells. Uptake by cells was measured using a Verse cytometer (BD, USA).

In order to visually observe the situation of the formulations entering the cell, the three Dex formulations labeled by PKH26 were incubated with resting or LPS-activated RAW264.7 cells for 2 h, then analyzed using confocal laser scanning microscopy (Leica SP8, Germany) after staining the cytoskeleton with FITC-phalloidin and the nucleus with DAPI[18].

2.10 Anti-inflammatory effects of nanoparticles to LPS-activated RAW264.7 cells

RAW264.7 cells were seeded into a 24-well plate at a density of 5×10^5 cells per well and allowed to adhere, then stimulated for 24 h with LPS at a final concentration of 100 ng/mL. The medium was replaced with fresh medium containing FPC-Exo/Dex, Exo/Dex, Lip/Dex or free Dex at a final Dex concentration of 20 μg/mL. Negative control wells were incubated in culture contain PBS. After 24 h, the culture medium was collected, centrifuged at 2000 *g* for 5 min, and the supernatant was assayed for IL-β, TNF-α and IL-10 using ELISA kits according to the manufacturer's instructions [21].

2.11 Establishing Mouse model of collagen-induced arthritis (CIA)

Bovine type II collagen was thoroughly emulsified with an equal volume of complete Freund's adjuvant by vortex, and 100 μL of emulsion was administered intradermally at the base of the mouse tail. After 21

days, mice received an intradermal booster injection of type II collagen with an equal volume of incomplete Freund's adjuvant.

2.12 Biodistribution of nanoparticles in CIA mice

A total of 12 CIA mice were randomly divided into 4 groups (3 animals per group), which were intravenously administered DID-labeled Lip/Dex, Exo/Dex, FPC-Exo/Dex, or free DID (1 μg DID per mouse). At 1, 4, 8, and 24 h later, mice were anesthetized with 10% chloral hydrate (0.04 mL per 10 g) and analyzed using the IVIS® Spectrum system (Caliper, Hopkinton, MA, USA).

At 24 h, mice were euthanized and the blood, heart, liver, spleen, lung, and kidney were removed. Blood was sampled and centrifuged at 3000 *g* for 7 min to obtain plasma. Fluorescence of plasma and organs was measured using the IVIS® Spectrum system (PerkinElmer, USA).

2.13 Measurement of weight, paw thickness, foot volume and articular index (AI) score of CIA mice

On day 21 after the booster immunization, CIA mice were randomly assigned to five groups (3 animals per group) and injected intravenously with free Dex, Lip/Dex, Exo/Dex or FPC-Exo/Dex at a Dex dose of 1.2 mg/kg in all cases. Negative control mice were injected with the same volume of Saline. AI scores were determined for each limb as described [8]. Body weight, hind paw thickness and foot volume were measured every 3 days during treatment. Foot volume is measured with drainage method.

2.14 Micro-computed tomography (Micro-CT) analyses of articular bone

After mice were sacrificed, the left hind limbs were removed and immediately fixed in 4% paraformaldehyde for 48 h. Then the microstructure of each limb was analyzed using a SIEMENS Inveon PET/CT computed tomography system (SIEMENS, Germany) with the following parameters: voltage, 80 kV; current, 500 μA; exposure time, 1800 ms; total rotation, 220°; and projections, 120 sheets. A region of interest (ROI) of the trabecular bone within the calcaneus was defined by aligning the calcaneus bone along the sagittal plane using the Data Viewer, starting 0.2 mm away from the epiphyseal plate and continuing for 40–50 slides (1 mm)[30, 31]. The bone mineral density (BMD), percent bone volume (BV/TV), bone surface density (BS/BV), trabecular thickness (Tb.Th), trabecular number (Tb.N) and trabecular spacing (Tb.Sp) of the ROI were calculated using SIEMENS Inveon Research Workplace software 4.2.

2.15 Histological evaluation of joint tissues

Ankle joints were dissected from each group, fixed in 4% paraformaldehyde for 48 h, and decalcified in 10% neutral EDTA solution for 15 days at room temperature. Then decalcified tissue was embedded in paraffin. Thin sections (5 μm) were cut and stained with hematoxylin-eosin (H&E) or safranin O (SO) combines with chondroitin sulfate to stain articular cartilage red [32]. An H&E score from 0 to 3 was determined for each of the following aspects: inflammatory cell infiltration, synovial tissue proliferation, fibrous tissue hyperplasia, and macrophage infiltration. Then all these scores were summed for a given

ankle joint, and the overall scores for all ankle joints were summed to obtain H&E scores for a given animal.

2.16 Evaluation of inflammatory cytokines in serum

Blood samples and joint tissues were collected from mice on day 45 after induction of CIA. Serum levels of inflammatory cytokines TNF-α, IL-1β and IL-10 were measured using ELISA kits according to the manufacturer's instructions.

2.17 In vivo safety evaluation of nanoparticles in CIA mice

Aspartate transaminase (AST) and alanine transaminase (ALT) levels of serum collecting from different treatment groups were assayed using a commercial kit (Nanjing Institute of Biological Engineering, Nanjing, China) according to the manufacturer's protocol.

2.18 Statistical analysis

Statistical analysis was performed using Graphpad Prism 6.0 (GraphPad Software, La Jolla, CA, USA). Statistical comparisons were performed by one-way ANOVA (Dunnett's multiple comparisons test) for multiple groups, except for the analyses in Fig. 4B and Fig. 6B, which were performed using two-way ANOVA. Differences associated with $p < 0.05$ were considered significant. All results were expressed as mean ± SD.

3. Results

3.1 Characterization of exosomes

Exosomes (Exos) showed an average size of 98.87 ± 6.69 nm, PDI of 0.36 ± 0.01, and zeta potential of -12.03 ± 1.47 mV (Fig. 1A-B). Consistent with these results, transmission electron microscopy displayed that exosomes were round-shaped nanovesicles surrounded by membrane, with a diameter of approximately 100 nm (Fig. 1C). Ultimately, 2.20 ± 0.44 μg of exosomes (based on protein content) could be purified from 1 mL of culture medium. Western blot experiments showed that the exosomes contained the marker proteins CD9 and CD63 (Fig. 1D).

3.2 Structure of FA-NHS and FA-PEG-Chol

^{1}H-NMR showed signals at 6.93 ppm and 7.60 ppm belonging to the *para*-aminobenzoic acid moiety in FA, as well as signals at 4.21–4.30, 1.79–2.05 and 2.20–2.31 ppm belonging to the α-, β-, and γ-CH_2-protons of the glutamic acid moiety of FA (Fig. S1). The signal at 2.44–2.49 ppm was attributed to the proton of the NHS group.

^{1}H-NMR of FA-PEG-Chol confirmed the formation of the conjugate, showing principal peaks related to FA (8.53–8.78, 7.73–7.65, 5.60–5.52, 4.64–4.53 ppm), the PEG moiety (3.46–3.64 ppm) and the Chol

moiety (0.86 – 0.82, 0.62–0.69 ppm) (Fig.S 2).

3.3 Characterization of different Dex preparations and incorporation of FA-PEG-Chol into Exo/Dex

Average diameter was smallest for Exo/Dex (106.27 ± 11.40 nm), intermediate for Lip/Dex (112.60 ± 10.61 nm) and largest for FPC-Exo/Dex (128.43 ± 16.27 nm) (Fig. 2A-D). Nevertheless, the three formulations did not differ significantly in size. Zeta potential was − 34.80 ± 6.60 mV for Exo/Dex, -11.00 ± 0.61 mV for Lip/Dex and − 22.73 ± 0.91 mV for FPC-Exo/Dex (Fig. 2A). PDI was approximately 0.3 for all three formulations, indicating narrow size distribution. Transmission electron microscopy showed that Exo/Dex, FPC-Exo/Dex and Lip/Dex all exhibited typical sphere-like shapes (Fig. 2E-G). We used UV spectroscopy to determine that 21.37 ± 5.46 μg of FA was incorporated into 100 μg of exosomes.

Exo/Dex showed EE of 11.12 ± 1.82% and DLE of 22.38 ± 1.13%. The corresponding values for FPC-Exo/Dex were lower (10.26 ± 0.73% and 18.81 ± 2.05%), as were the values for Lip/Dex (83.36 ± 1.43% and 13.54 ± 2.09%) (Fig. 2A).

3.4 *In vitro* cumulative drug release and toxicity of nanoparticles

Dex was released from FPC-Exo/Dex in a slow, sustained fashion (Fig. 3A). During the first 8 h, only 47.26% of Dex was released from FPC-Exo/Dex, compared to 90.46% of Dex from the free drug solution. Drug release from Exo/Dex and Lip/Dex was intermediate between these two extremes.

Exposing HUVEC cultures for 24 h to free Dex or any of the Dex-loading formulations had no obvious effect on viability, which remained above 80% even at a concentration of 25 μg/mL (Fig. 3B). When we performed these toxicity experiments on RAW264.7 cultures, we found no significant decrease in viability with FPC-Exo/Dex, and a slight decrease with free Dex (Fig. 3C).

3.5 Cellular uptake of nanoparticles by RAW264.7 cells

RAW264.7 cells internalized larger amounts of Dex formulations after activation with LPS, especially the largest of FPC-Exo/Dex (Fig. 4A-B). Regardless of activation status, cells took up more FPC-Exo/Dex than the other Dex formulations. Moreover, the endocytosis of Exo/Dex was more than Lip/Dex. These flow cytometry results were supported by confocal imaging (Fig. 4C-D). Confocal images instruct that FPC-Exo/Dex entered the cytoplasm the most, followed by Exo/Dex. Especially in LPS-activated RAW264.7 cells.

3.6 Effect to inflammatory cytokines secretion

TNF-α levels in culture medium were much lower after LPS-activated RAW264.7 cells were treated with FPC-Exo/Dex and Exo/Dex than with free Dex or Lip/Dex (Fig. 5A). Similarly, the formulations inhibited secretion of IL-1β, with FPC-Exo/Dex showing a stronger effect, then followed by Exo/Dex (Fig. 5B), suggesting that the exosome-based drug delivery system exerts better anti-inflammatory effects. FPC-

Exo/Dex significantly up-regulated the anti-inflammatory cytokine IL-10 ($p < 0.01$), Exo/Dex also did ($p < 0.05$) (Fig. 5C).

3.7 Biodistribution of nanoparticles in CIA mice

Real-time fluorescence imaging revealed that all three DID-labeled preparations accumulated in the joints of CIA mice at 1 h (Fig. 6A), presumably due to the ELVIS effect. DID/FPC-Exo/Dex showed the greatest accumulation into joints at every time points. Even at 24 h, the DID/FPC-Exo/Dex group showed intensive fluorescence, whereas the DID/Lip/Dex group showed slight signal by 8 h (Fig. 6A). Semi-quantitation of fluorescence intensity in ankle joints further indicate that DID/FPC-Exo/Dex group displayed more significant fluorescence than other groups (Fig. 6C). In addition, DID/Exo/Dex group displayed significantly fluorescence at 4, 8 and 24 h compare to DID/Lip/Dex group (Fig. 6C). These results suggest that FPC-Exo/Dex may target inflammatory lesions better and persist there longer than Exo/Dex and Lip/Dex, and Exo/Dex showed better targeting performance than Lip/Dex. *Ex vivo* imaging indicated that DID/FPC-Exo/Dex accumulated more in plasma than other groups after 24 h, suggesting its long systemic circulation (Fig. 6B,D). Furthermore, obvious fluorescence was detected in livers of all groups, however, DID/FPC-Exo/Dex group had lower distribution than Exo/Dex (Fig. 6B,D), suggesting modifying with FPC could decrease non-specific distribution. Fluorescence in spleens and lungs was faint, almost no fluorescence was detected in kidney (Fig. 6B,D).

3.8 Therapeutic efficacy in CIA mice based on body weight, AI scores, paw thickness and foot volume

Body weight serves as an indirect indicator of therapeutic efficacy in RA since disease progression is associated with weight loss due to less feeding and greater apathy [33]. Body weight in mice injected with FPC-Exo/Dex increased continuously from day 21 (2nd booster injection) until day 45, and it had no significant difference with Normal group (Fig. 7A). All treatment groups showed an initial increase in scores, reflecting disease progression, followed by a decrease in scores, reflecting therapeutic effects (Fig. 7B). FPC-Exo/Dex was associated with the lowest AI scores (Fig. 7B). This formulation also led to the least swelling of the hind limbs, based on paw thickness and foot volume, followed by Exo/Dex (Fig. 7C-D).

Imaging of the left hind limbs in animals treated with saline showed severe, extensive joint swelling and joint deformation, which free Dex reduced slightly but not markedly (Fig. 7E). FPC-Exo/Dex reduced this swelling nearly completely, such that the difference from saline-treated animals was not significant. Exo/Dex also significantly ameliorated swelling, but not as much as FPC-Exo/Dex.

3.9 Microstructure of articular bone based on Micro-CT

Saline-treated animals showed the most severe damage, with extensive erosion of the bone in ankle and toe joints (Fig. 8A). FPC-Exo/Dex was associated with significantly lower ankle bone erosion, which was no longer obvious after four times administrations. Quantitative analysis of the ROI in calcaneus showed that FPC-Exo/Dex treatment preserved the bone quality as evident in the morphometric parameters, such

as bone mineral density (BMD), percent bone volume (BV/TV), bone surface density (BS/BV), trabecular thickness (Tb.Th), trabecular number (Tb.N) and trabecular spacing (Tb.Sp), with their values similar to those observed for healthy controls; significantly better than those observed for other Dex formulations treated groups (Fig. 8B-G). Meanwhile, the values of BMD, BV/TV, BS/BV and Tb.Th in Exo/Dex-treated group are significantly lower than these of Lip/Dex-treated groups, and Exo/Dex-treated group displayed a slightly lower articular bone erosion.

3.10 Histological analysis of joint tissue

Compared to healthy control animals, H&E staining of histology slices from CIA mice treated with saline or free Dex revealed marked inflammatory cell infiltration, synovial tissue expansion and fibrous tissue hyperplasia (Fig. 9A). Average histopathology scores were 7.0 in the Saline group and 6.0 in the Dex-treated group. Animals treated with Lip/Dex showed a score of 4.3, indicating moderate damage. The corresponding scores in the Exo/Dex and FPC-Exo/Dex groups were 2.3 and 0.7, indicating markedly reduced joint damage of FPC-Exo/Dex (Fig. 9C).

Based on SO staining, articular cartilage was nearly destroyed in animals treated with saline or free Dex (Fig. 9B), and the destruction was significantly less severe in animals treated with FPC-Exo/Dex. In addition, joints from animals treated with Lip/Dex showed weaker red staining on articular surfaces than Exo/Dex-treated animals, suggesting severer degradation and destruction of articular cartilage tissue.

3.11 Inflammatory Cytokines in serum of CIA mice after treatment

Following CIA induction, levels of both IL-1β and TNF-α in the serum increased, and these increases were marginally but not significantly smaller with free Dex or Lip/Dex, while significantly smaller with FPC-Exo/Dex ($p < 0.01$) and Exo/Dex ($p < 0.05$) (Fig. 10A-B). In addition, the level of IL-1β in Exo/Dex-treated group is lower than it of Lip/Dex-treated group. Meanwhile, FPC-Exo/Dex treatment increased the level of IL-10 the most in all groups ($p < 0.001$), then Exo/Dex ($p < 0.01$) (Fig. 10C).

3.12 Hepatotoxicity analysis of nanoparticles in CIA mice after treatment

Serum levels of AST and ALT in any of the Dex-treated groups were not significantly different from those in the healthy, untreated controls (Fig. 11), indicating that this therapeutic strategy may not cause obvious damage to the liver. FPC-Exo/Dex was associated with marginally but not significantly levels of both indices than free Dex (Fig. 11). These results suggest desirable biocompatibility of FPC-Exo/Dex *in vivo*.

4. Discussion

In this study, we derived the exosomes from RAW264.7 macrophages, because inflammatory lesions in RA contain abundant activated macrophages, and cells appear to internalize exosomes better when those exosomes were derived from the same cell type [26, 34–36]. At the same time, it was reported that

exosomes derived from macrophages have achieved excellent therapeutic efficacy in the treatment of other inflammations [20, 22] Therefore, the choice of macrophages as the donor cell of exosomes is cogitative. Ultracentrifugation was used to extracted exosomes, for this classical approach may extract exosomes more efficiently and provide better dispersity than other extraction methods [37, 38]. But ultracentrifugation takes a long time, considering that our research needs to extract a large amount of exosomes, an additional ultrafiltration procedure was added to concentrate the volume of the medium before the ultracentrifugation. Dynamic light scattering showed the resulting exosomes to be uniformly disperse in the narrow range of 80–100 nm, and a protein assay estimated a yield of 2.20 ± 0.44 μg of exosomes from 1 mL of culture medium. These results indicate that our combination of ultrafiltration and ultracentrifugation is suitable for the extraction of exosomes from RAW264.7 cells with adequate yields for subsequent experiments.

Electroporation is widely used to load chemical drug, short interfering RNA and DNA into exosomes [39]. But, exosomes are tend to aggregate during electroporation [40].Therefore, we included 80 mM trehalose in the mixture of Dex and exosomes during electroporation to prevent aggregation of the exosomes [41], which may help explain why we obtained a uniform dispersion of size with narrow PDI.

We modified the exosomes with FA-PEG-Chol compound to optimize their properties for better treating of RA. PEG can enhance stability and long circulation time of drug delivery system [42], and both the PEG and Chol help solubilize the FA and ensure its stable incorporation into the membrane of the exosomes. *In vitro* cumulative drug release study indicated that Dex was released more sustainably from FPC-Exo/Dex, verifying that the introduction of PEG can increase the stability of Exo/Dex. Biodistribution examination further showed that FPC-Exo/Dex was retained more and longer in joint tissues than Exo/Dex in CIA mice, and this is not only related to the active targeting ability which was brought by the FA modification, but also to the fact that PEG can prolong circulation time. These results confirm that “FPC” modification of nanoparticles ensured their active targeting to inflammatory sites in RA, and exosomes exhibits favourable stability and circulation *in vivo*. Consistent with this, cellular uptake studies also indicted that FPC-Exo/Dex was taken up by LPS-activated macrophages to a greater extent, followed by Exo/Dex.

The results of evaluation the effect of nanoparticles on inflammatory cytokines *in vitro* and in *vivo*, indicated that FPC-Exo/Dex inhibited pro-inflammatory cytokines and promoted production of anti-inflammatory cytokine IL-10 to the greatest extent. Exo/Dex also behaved better than Lip/Dex. Therapeutic efficacy study in *vivo* found that FPC-Exo/Dex triggered these therapeutic effects in CIA mice to a significantly greater extent than other Dex formulations. These effects correlated with significantly lower histopathology scores based on H&E staining, significantly less cartilage and articular bone destruction based on SO staining and Micro-CT. The less severe bone destruction may be an indirect results of the ability of FPC-Exo/Dex (a) to reduce secretion of IL-1β and TNF-α, since these factors may promote the formation of osteoclasts [43–45]; and (b) promote secretion of IL-10, which can inhibit osteoclast formation. The superior therapeutic effects of FPC-Exo/Dex over the other Dex formulations may relate to its better targeting and internalization.

FPC-Exo/Dex showed good biocompatibility not only in culture studies with HUVEC and RAW264.7 cells but also in mice. Since exosomes tend to accumulate in the liver and our biodistribution assay showed substantial accumulation of Dex preparation in liver, we analyzed effects of Dex treatment on liver function, based on AST and ALT. FPC-Exo/Dex was associated with similar values as in healthy, untreated controls, suggesting that Dex-loaded exosomes are biocompatible.

Results of comparative research between Exo/Dex and Lip/Dex suggest that exosome-based on drug delivery system had better internalization, weaker blood clearance and long-term circulating capability. Consistently, Exo/Dex displayed better therapeutic efficacy than Lip/Dex, reflecting the advantages of exosome as an endogenous nanocarrier over liposome.

In summary, exosome is an idea nanocarrier to delivery GCs for treatment to RA, and with proper modification, it can exert better therapeutic efficacy. However, the encapsulation efficiency of exosome-based drug system is mostly less than 30% [22, 46], it is also relatively low in our study. But the encapsulation efficiency in physical nanoparticles is almost over 90% [8, 47]. With the research progressed, it has been reported that encapsulating drug-loading physical nanoparticles into exosomes to enhance the encapsulation efficiency of drug delivery system and take endogenous advantage of exosomes [48, 49]. Our future research could be enhanced by combined with these latest developments.

5. Conclusion

We prepared relatively simple, biocompatible FPC-Exo/Dex nanoparticles as a drug delivery platform. These particles show the advantages of other formulations as well as greater stability and longer persistence because of their PEG-Chol-FA modification. These modified exosomes were endocytosed better *in vitro* than Exo/Dex, or free Dex, and they targeted inflamed joints and protected bone and cartilage better in mice with collagen-induced arthritis. They down-regulated the levels of pro-inflammatory cytokines and up-regulated anti-inflammatory cytokine, strongly inhibiting macrophage-driven inflammation in CIA mice. The FPC-Exo/Dex system constructed in our study may be a useful drug delivery system for GCs to treat RA.

Abbreviations

GCs: glucocorticoids; RA: rheumatoid arthritis; Exo: exosome; FA: folic acid; Dex: dexamethasone sodium phosphate; PEG: polyethylene glycol; Chol: cholesterol; ELISA: enzyme-linked immunosorbent assay; CIA: collagen-induced arthritis; EE: encapsulation efficiency; DLE: drug loading efficiency; ELVIS: extravasation through leaky vasculature and subsequent inflammatory cell-mediated sequestration; Lip: liposome; PDI: polydispersity index; TEM: transmission electron microscopy; HUVEC: human umbilical vein endothelial cells; MTT: 3-(4,5dimethylthiozol-2-yl)-2,5-diphenyl-tetrazolium bromide; LPS: lipopolysaccharide; Micro-CT: micro-computed tomography; DID: 1,1'-Dioctadecyl-3,3,3',3'-etramethylindodicarbocyanine perchlorate; AI: articular index; H&E: hematoxylin-eosin staining; SO: safranin O staining; AST: aspartate aminotransferase; ALT: alanine transaminase.

Declarations

Ethics approval and consent to participate

Not applicable for this study.

Consent for publication

We give our consent for the manuscript to be published in Journal of Nanobiotechnology.

Availability of data and materials

All data generated or analyzed during this study are included in this article.

Conflicts interests

The authors declare that they have no competing interests

Funding

This work was supported by the National Natural Science Foundation of China (grant numbers 81803478, 2018); Science and Technology Project of Luzhou Government (grant numbers 2019-JYJ-51, 2019); Sichuan Science and Technology Program (grant numbers 2017RZ0048, 2017); Science and Technology Project of the Health Planning Committee of Sichuan (grant numbers ZD18036, 2018); and the Transformation Project of Science and Technology Achievements of Southwest Medical University (grant numbers 2018002, 2018).

Acknowledgements

All authors are thankful for getting help and supports from the following research platforms, the Key Laboratory of Medical Electrophysiology of Ministry of Education, the Experimental Center of Basic Medicine, School of Pharmacy, Southwest Medical University, Luzhou, Sichuan 646000, China.

Author contributions

YF and CL conducted most of the research and wrote the manuscript. LH, F Y and CX helped with the experiment. MZ and YW participated in discussions. ZZ and LC guided the entire study and edited the manuscript.

References

1. Prasad LK, O'Mary H, Cui Z. Nanomedicine delivers promising treatments for rheumatoid arthritis. Nanomed. 2015; 10: 1-12.
2. Quan L, Zhang Y, Crielaard BJ, Dusad A, Lele SM, Rijcken CJF, Metselaar JM, Kostkova H, Etrych T, Ulbrich K, etal. Nanomedicines for Inflammatory Arthritis: Head-to-Head Comparison of Glucocorticoid-Containing Polymers, Micelles, and Liposomes. ACS Nano. 2014; 8: 458-466
3. Wang Q, Sun X. Recent advances in nanomedicines for the treatment of rheumatoid arthritis. Biomater Sci. 2017; 5: 1407-1420.
4. Leblond A, Allanore Y, Avouac J. Targeting synovial neoangiogenesis in rheumatoid arthritis. Autoimmun Rew. 2017; 16: 594-601.
5. Wang Q, Jiang H, Li Y, Chen W, Li H, Peng K, Zhang Z, Sun X. Targeting NF-kB signaling with polymeric hybrid micelles that co-deliver siRNA and dexamethasone for arthritis therapy. Biomaterials. 2017; 122: 10-22.
6. Barnes PJ. Anti-inflammatory Actions of Glucocorticoids: Molecular Mechanisms. Clin Sci. 1998; 94: 557-572.
7. Vandewalle J, Luypaert A, Bosscher KD, Libert C. Therapeutic Mechanisms of Glucocorticoids. Trends Endocrinol Metab. 2017; 29: 42-54.
8. Wang Q, Jiang J, Chen W, Jiang H, Zhang Z, Sun X. Targeted delivery of low-dose dexamethasone using PCL–PEG micelles for effective treatment of rheumatoid arthritis. JCR. 2016; 230: 64-72.
9. Wang Y, Liu Z, Li T, Chen L, Lyu J, Li C, Lin Y, Hao N, Zhou M, Zhong Z. Enhanced Therapeutic Effect of RGD-Modified Polymeric Micelles Loaded With Low-Dose Methotrexate and Nimesulide on Rheumatoid Arthritis. Theranostics. 2019; 9: 708-720.
10. Li C, Li H, Wang Q, Zhou M, Li M, Gong T, Zhang Z, Sun X. pH-sensitive polymeric micelles for targeted delivery to inflamed joints. JCR. 2017; 246: 133-141.
11. Zhou M, Hou J, Zhong Z, Hao N, Lin Y, Li C. Targeted delivery of hyaluronic acid-coated solid lipid nanoparticles for rheumatoid arthritis therapy. Drug Deliv. 2018; 25: 716-722.
12. Li C, Wang J, Wang Y, Gao H, Wei G, Huang Y, Yu H, Gan Y, Wang Y, Mei L, Chen H, Hu H, Zhang Z, Jin Y. Recent progress in drug delivery. Acta Pharm Sin B. 2019; 9: 1145-1162.
13. Holland CK, Mcpherson DD. Echogenic Lipsomes for Targeted Drug Delivery. Proc IEEE Int Symp Biomed Imaging. 2009; 29: 755-758.
14. Torchilin VP, Affinity Lipsomes In Vivo: Factors Influencing Target accumulation, J Mol Recognit. 1996; 9: 335-346.

15. Wu G, Zhang J, Zhao Q, Zhuang W, Ding J, Zhang C, Gao H, Pang D, Pu K, Xie H. Molecularly Engineered Macrophage-Derived Exosomes with Inflammation Tropism and Intrinsic Heme Biosynthesis for Atherosclerosis Treatment. Angew Chem Int Ed Engl. 2020; 59: 4068-4074.
16. Koenders MI, VandenBerg WB. Novel therapeutic targets in rheumatoid arthritis. Trends Pharmacol Sci. 2015; 36: 189-195.
17. Bunggulawa EJ, Wang W, Yin T, Wang N, Durkan C, Wang Y, Wang G. Recent advancements in the use of exosomes as drug delivery systems. J Nanobiotechnol. 2018; 16: 81-94
18. Qu M, Lin Q, Huang L, Fu Y, Wang L, He S, Fu Y, Yang S, Zhang Z, Zhang L, Sun X. Dopamine-loaded blood exosomes targeted to brain for better treatment of Parkinson's disease. JCR. 2018; 287: 156-66.
19. Haney MJ, Klyachko NL, Zhao Y, Gupta R, Plotnikova EG, He Z, Patel T, Piroyan A, Sokolsky M, Kabanov AV, Batrakova EV. Exosomes as drug delivery vehicles for Parkinson's disease therapy. JCR. 2015; 207: 18-30.
20. Yuan D, Zhao Y, Banks WA, Bullock KM, Haney M, Batrakova E, Kabanov AV. Macrophage exosomes as natural nanocarriers for protein delivery to inflamed brain. Biomaterials. 2017; 142: 1-12.
21. Lin Q, Qu M, Zhou B, Patra HK, Sun Z, Luo Q, Yang W, Wu Y, Zhang Y, Li L,etal. Exosome-like nanoplatform modified with targeting ligand improves anti-cancer and anti-inflammation effects of imperialine. JCR.2019; 311: 104-116.
22. Tang TT, Lv LL, Wang B, Cao JY, Feng Y, Li ZL, LI ZL, Wu M, Wang FM, Wen Y, etal. Employing Macrophage-Derived Microvesicle for Kidney-Targeted Delivery of Dexamethasone: An Efficient Therapeutic Strategy against Renal Inflammation and Fibrosis. Theranostics. 2019; 9: 4740-4755.
23. Malhi SS, Budhiraja A, Arora S, Chaudhari KR, Nepali K, Kumar R, Sohi H, Murthy RSR. Intracellular delivery of redox cycler-doxorubicin to the mitochondria of cancer cell by folate receptor targeted mitocancerotropic liposomes. Int J Pharm. 2012; 432: 63-74.
24. Thomas TP, Goonewardena SN, Majoros IJ, Kotlyar A, Cao Z, Leroueil PR, Baker JR. Folate-targeted nanoparticles show efficacy in the treatment of inflammatory arthritis. Arthritis Rhe 2011; 63: 2671-2780.
25. Kinne RW, Bräuer R, Stuhlmüller B, Palombo-Kinne E, Burmester G-R. Macrophages in rheumatoid arthritis. Arthritis Res Ther. 2000; 2: 189.
26. Chiba, Mitsuru. Exosomes secreted from human colorectal cancer cell lines contain mRNAs, microRNAs and natural antisense RNAs, that can transfer into the human hepatoma HepG2 and lung cancer A549 cell lines. Oncol Rep. 2012; 28: 1551-1558.
27. Siafaka P, Betsiou M, Tsolou A, Angelou E, Bikiaris DJJoMSMiM. Synthesis of folate-pegylated polyester nanoparticles encapsulating ixabepilone for targeting folate receptor overexpressing breast cancer cells. Deliv sys. 2015; 26: 275-289.
28. Saul JM, Annapragada A, Natarajan JV, Bellamkonda RV. Controlled targeting of liposomal doxorubicin via the folate receptor in vitro. JCR. 2003; 92: 49-67.

29. Yang KK, Kong M, Wei YN, Liu Y, Cheng XJ, Li J, Park HJ, Chen XG. Folate-modified–chitosan-coated liposomes for tumor-targeted drug delivery. J Mater Sci. 2013; 48: 1717-1728.
30. Quan L, Zhang Y, Dusad A, Ren K, Purdue PE, Goldring SR, Wang D. The Evaluation of the Therapeutic Efficacy and Side Effects of a Macromolecular Dexamethasone Prodrug in the Collagen-Induced Arthritis Mouse Model. Pharm Res. 2016; 33: 186-193.
31. Wu J, Xin W, Gang Z, Josselyn G, M. LS, Xiaoyan W, Liu Y, Dhruvkumar MS, Purdue PE, Mikuls TR, Goldring SR, Wang D. Development of a Janus Kinase (JAK) Inhibitor Prodrug for the Treatment of Rheumatoid Arthritis. Mol Pharm. 2018; 15: 456-3467
32. Reumson A, Kim DY, Hun PS, Yong J, Kim K, Ju KB, Yin XY, Kim JH, Min BH, Han DK, Kim MS. Direct chemotherapeutic dual drug delivery through intra-articular injection for synergistic enhancement of rheumatoid arthritis treatment. Sci Rep. 5: 147-153.
33. Crielaard BJ, Rijcken CJF, Quan L, Vander WS, Altintasl, Pot MVD, Kruijtzer JAW, Liskamp RMJ, Schiffelers RM, Nostrum CFV, Glucocorticoid-Loaded Core-Cross-Linked Polymeric Micelles with Tailorable Release Kinetics for Targeted Therapy of Rheumatoid Arthritis. Angew. Chem Int. Ed. Engl. 2012; 51: 7254-7258.
34. Zhao L, Gu C, Gan Y, Shao L, Chen H, Zhu H. Exosome-mediated siRNA delivery to suppress postoperative breast cancer metastasis. JCR. 2020; 318: 1-15.
35. Beez CM, Haag M, Klein O, Sophie VL, Michael S, Martina S. Extracellular vesicles from regenerative human cardiac cells act as potent immune modulators by priming monocytes. J Nanobiotechnol. 2019; 17: 72-90.
36. Singh PP, Smith VL, Karakousis PC, Schorey JS. Exosomes Isolated from Mycobacteria-Infected Mice or Cultured Macrophages Can Recruit and Activate Immune Cells In Vitro and In Vivo. J Immunol. 2012; 189: 777-785.
37. Zhang Z, Wang C, Li T, Liu Z, Li L. Comparison of ultracentrifugation and density gradient separation methods for isolating Tca8113 human tongue cancer cell line derived exosomes. Oncol Lett. 2014; 8: 1701-1706.
38. Yamashita T, Takahashi Y, Nishikawa M, Takakura Y. Effect of Exosome isolation methods on physicochemical properties of exosomes and clearance of exosomes from the blood circulation. Euro J of Pharm Biopharm. 2015; 98: 1-8.
39. Lai RC, Yeo RWY, Tan KH, Lim SK. Exosomes for drug delivery—a novel application for the mesenchymal stem cell. Biotechnol Adv. 2012; 31: 543-551.
40. Johnsen KB, Gudbergsson JM, Skov MN, Christiansen G, Gurevich L, Moos T, Duroux M. Evaluation of electroporation-induced adverse effects on adipose-derived stem cell exosomes. Cytotechnology. 2016; 68: 2125-2138.
41. Hood JL, Scott MJ, Wickline SA. Maximizing exosome colloidal stability following electroporation. Anal Biochem. 2014; 448: 41-49.
42. Kooijmans SAA, Fliervoet LAL, van der Meel R, Fens MHAM, Heijnen HFG, van Bergen, Henegouwen PMP, Vader P, Schiffelers R M. PEGylated and targeted extracellular vesicles display enhanced cell

specificity and circulation time. JCR. 2016; 224: 77-85.

43. Ju J. Temporal differential effects of proinflammatory cytokines on osteoclastogenesis. Int J Mol Med.2013; 31: 769-777.
44. Pathak JL, Bravenboer N, Verschueren P, Lems WF, Luyten FP, Klein-Nulend J, Bakker AD. Inflammatory factors in the circulation of patients with active rheumatoid arthritis stimulate osteoclastogenesis via endogenous cytokine production by osteoblasts. Osteoporos Int. 2014; 25: 2453-2463.
45. Son HS, Lee J, Lee HI, Kim N, Jo YJ, Lee GR, et al. Benzydamine inhibits osteoclast differentiation and bone resorption via down-regulation of interleukin-1β expression. Acta Pharm Sin B. 2020; 10: 462-474.
46. Kim MS, Haney MJ, Zhao Y, Mahajan V, Batrakova EV. Development of Exosome-encapsulated Paclitaxel to Overcome MDR in Cancer cells. Nanomed. 2015; 12: 655-664.
47. Yan F, Li H, Zhong Z, Zhou M, Lin Y, Tang C, Li C. Co-Delivery of Prednisolone and Curcumin in Human Serum Albumin Nanoparticles for Effective Treatment of Rheumatoid Arthrit Int J Nanomedicine. 2019; 14: 9113-9125.
48. Liu C, Zhang W, Li Y, Chang J, Sun J. Microfluidic Sonication To Assemble Exosome Membrane-Coated Nanoparticles for Immune Evasion-Mediated Targeting. Nano Letters. 2019; 19: 7836-7844.
49. Petro Z, Alexander E , Thomas B , Anastasia M, Phil R ,Claudia M, Anja R, Yarua J, Achim A. Extracellular vesicle (ECV)-modified polyethylenimine (PEI) complexes for enhanced siRNA delivery in vitro and in vivo. JCR. 2020; 319: 63-76.

Figures

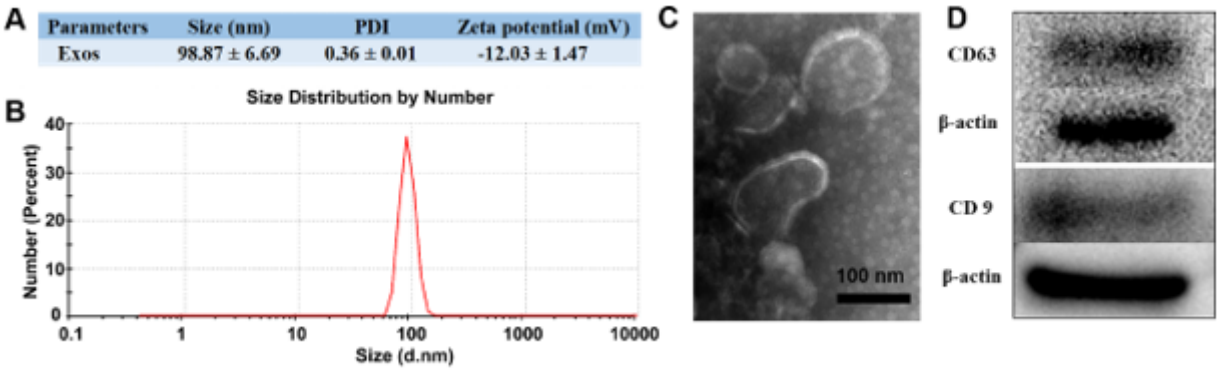

Figure 1

Characterization of exosomes. (A) Size, PDI and zeta potential of Exos. (B) Size distribution of Exos. (C) Transmission electron micrographs of Exos. (E) Western blot to confirm the expression of CD9 and CD63.

A

Nanoparticles	Size (nm)	PDI	Zeta potential (mV)	EE (%)	DLE (wt %)
Exo/Dex	106.27 ± 11.40	0.27 ± 0.04	-34.80 ± 6.60	11.12 ± 1.82	22.38 ± 1.13
FPC-Exo/Dex	128.43 ± 16.27	0.36 ± 0.05	-22.73 ± 0.91	10.26 ± 0.73	18.81 ± 2.05
Lip/Dex	112.60 ± 10.61	0.14 ± 0.03	-11.00 ± 0.61	83.36 ± 1.43	13.54 ± 2.09

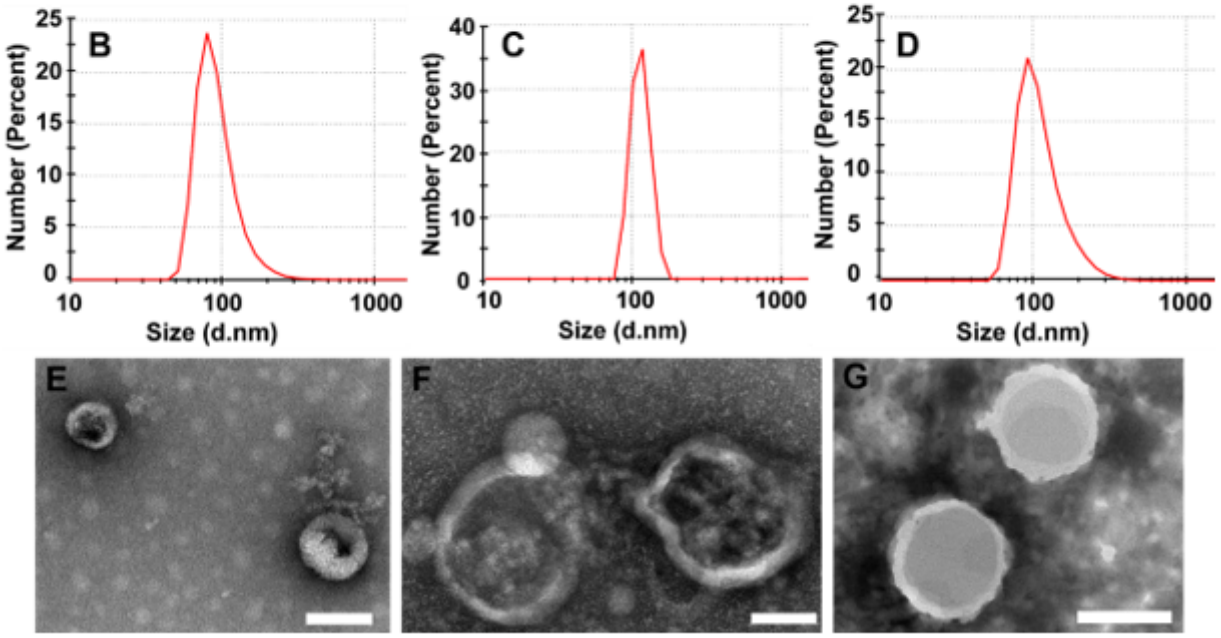

Figure 2

Characterization of Exo/Dex, FPC-Exo/Dex and Lip/Dex. (A) Size, PDI, zeta potential, EE and DLE of Dex preparations. Size distribution of Exo/Dex (B), FPC-Exo/Dex (C) and Lip/Dex (D). Transmission electron micrographs of Exo/Dex (E), FPC-Exo/Dex (F) and Lip/Dex.

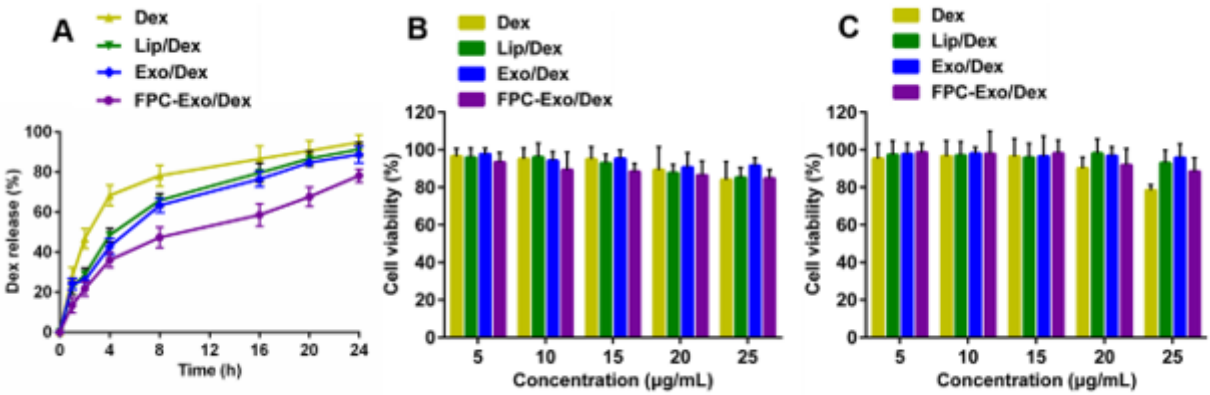

Figure 3

In vitro cumulative release and toxicity of Dex preparations. (A) Cumulative release of Dex from Lip/Dex, Exo/Dex and FPC-Exo/Dex (n = 3). The effect of Dex, Lip/Dex, Exo/Dex and FPC-Exo/Dex for HUVEC (B) and RAW264.7 cells viability (C). Data represent mean ± SD (n = 5).

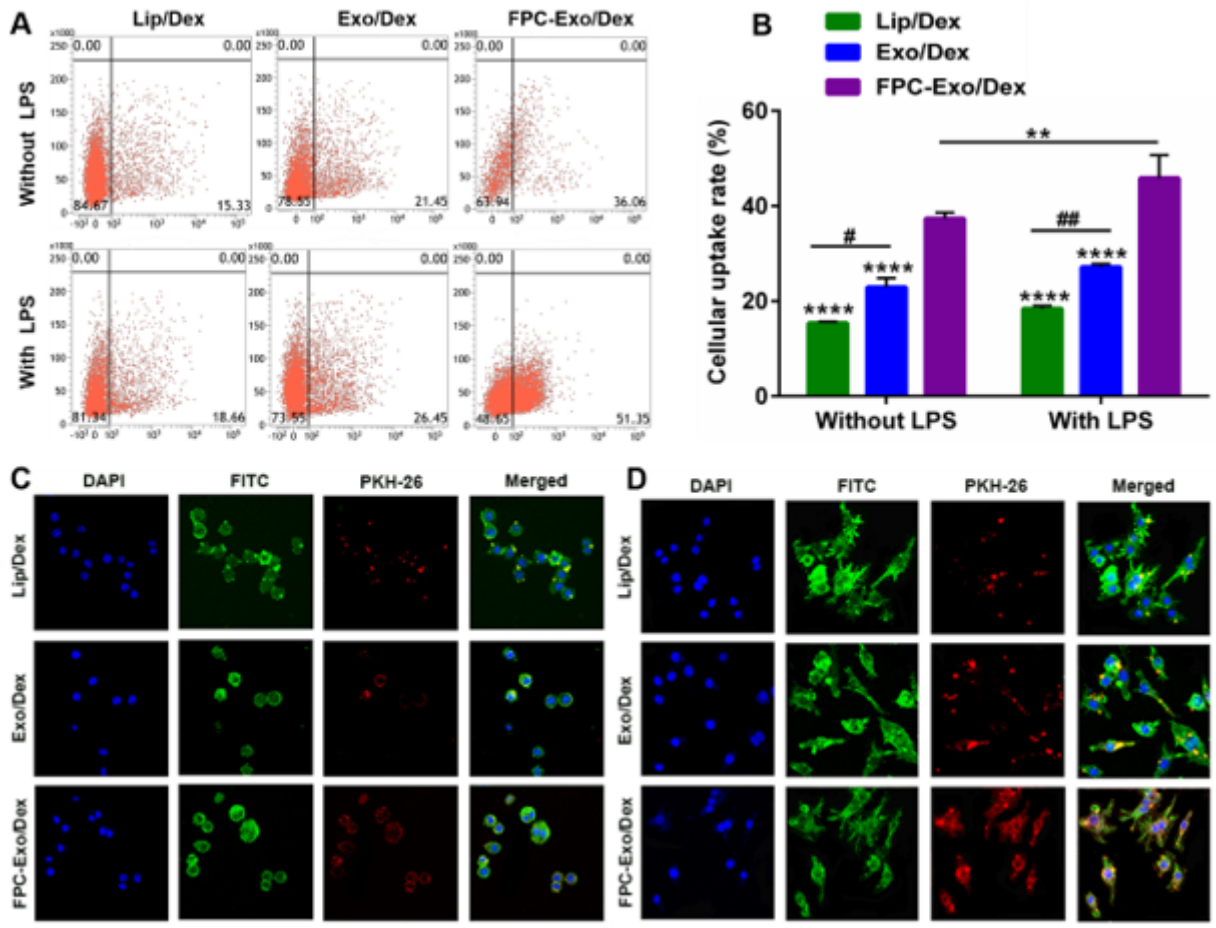

Figure 4

Uptake of Lip/Dex, Exo/Dex and FPC-Exo/Dex by RAW264.7 with or without LPS activation. (A) Representative images of Flow cytometry analysis showing uptake of Dex preparations labeled by PKH 67 in RAW264.7 cells with or without LPS activation. (B) Uptake rate of different Dex preparations by flow cytometry (n = 3, **p < 0.01, ****p < 0.0001 vs cells treated with FPC-Exo/Dex, #p < 0.05, ##p < 0.01 are cells treated with Lip/Dex compared to Exo/Dex). (C) Confocal microscopy showing uptake of different Dex preparations labeled by PKH 67 in RAW264.7 cells without LPS activation. Dex preparations appear in red; nucleus, blue; and cytoplasm, green. (D) Confocal microscopy showing uptake of different Dex preparations labeled by PKH 67 in RAW264.7 cells without LPS activation. Dex preparations appear in red; nucleus, blue; and cytoplasm, green.

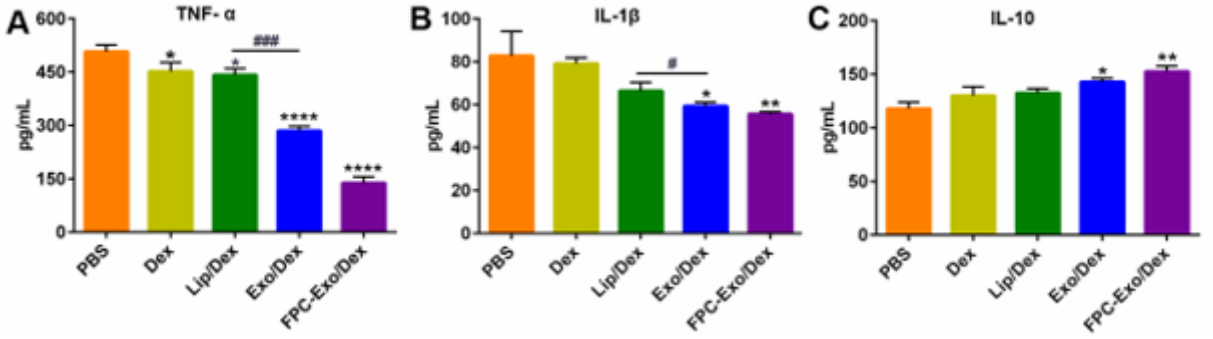

Figure 5

Expression of inflammatory cytokines in cell-free supernatants treated with different preparations. Level of (A) TNF- α, (B) IL-1β, and (C) IL-10 (n = 3, *p < 0.05, **p < 0.01, ***p < 0.001 vs cells treated with PBS, #p < 0.05, ###p < 0.001 are cells treated with Lip/Dex compared to Exo/Dex).

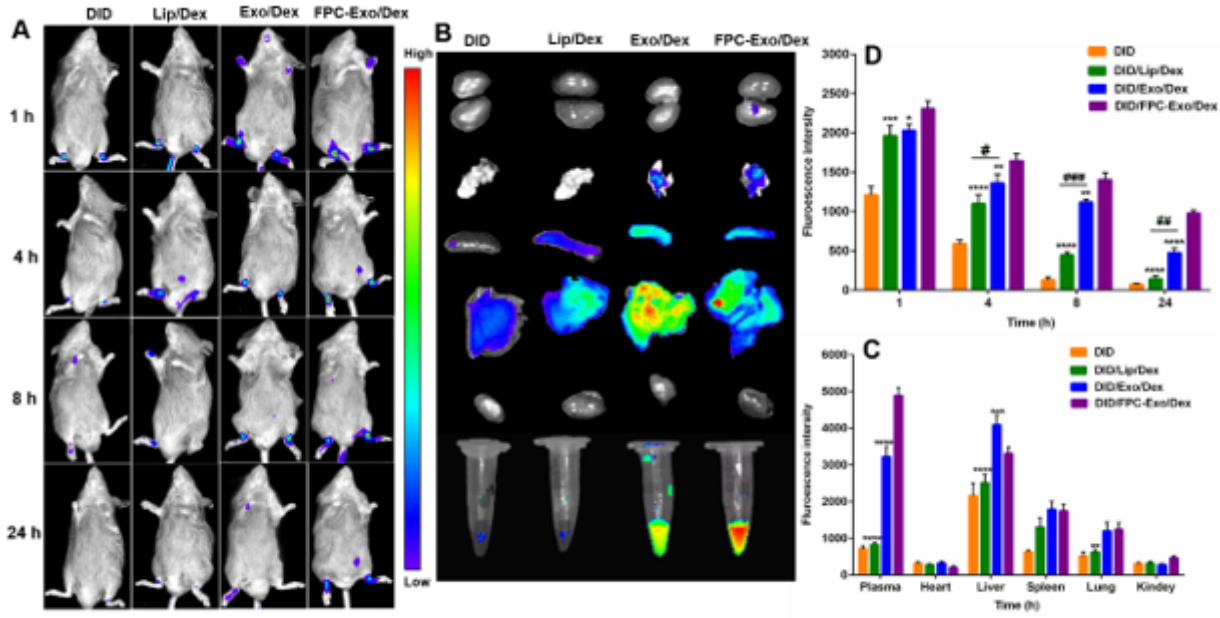

Figure 6

The real-time fluorescence imaging of CIA mice. (A) Real-time fluorescence imaging of CIA mice after intravenous injection with free DID, DID/Lip/Dex, DID/Exo/Dex and DID/FPC-Exo/Dex, respectively (n = 3). (B) Ex vivo imaging of the plasma and organs at 24 h after intravenous injection. (C) Semi-quantitation of fluorescence intensity in joints. (D) Semi-quantitation of fluorescence intensity in joints in plasma and organs (n = 3, *p < 0.05, **p < 0.01, ***p < 0.001, ****p < 0.0001 vs mice injectedted with DID/FPC-Exo/Dex, #p < 0.05, ##p < 0.01, ###p < 0.001 are mice injected with DID/Lip/Dex compared to DID/Exo/Dex).

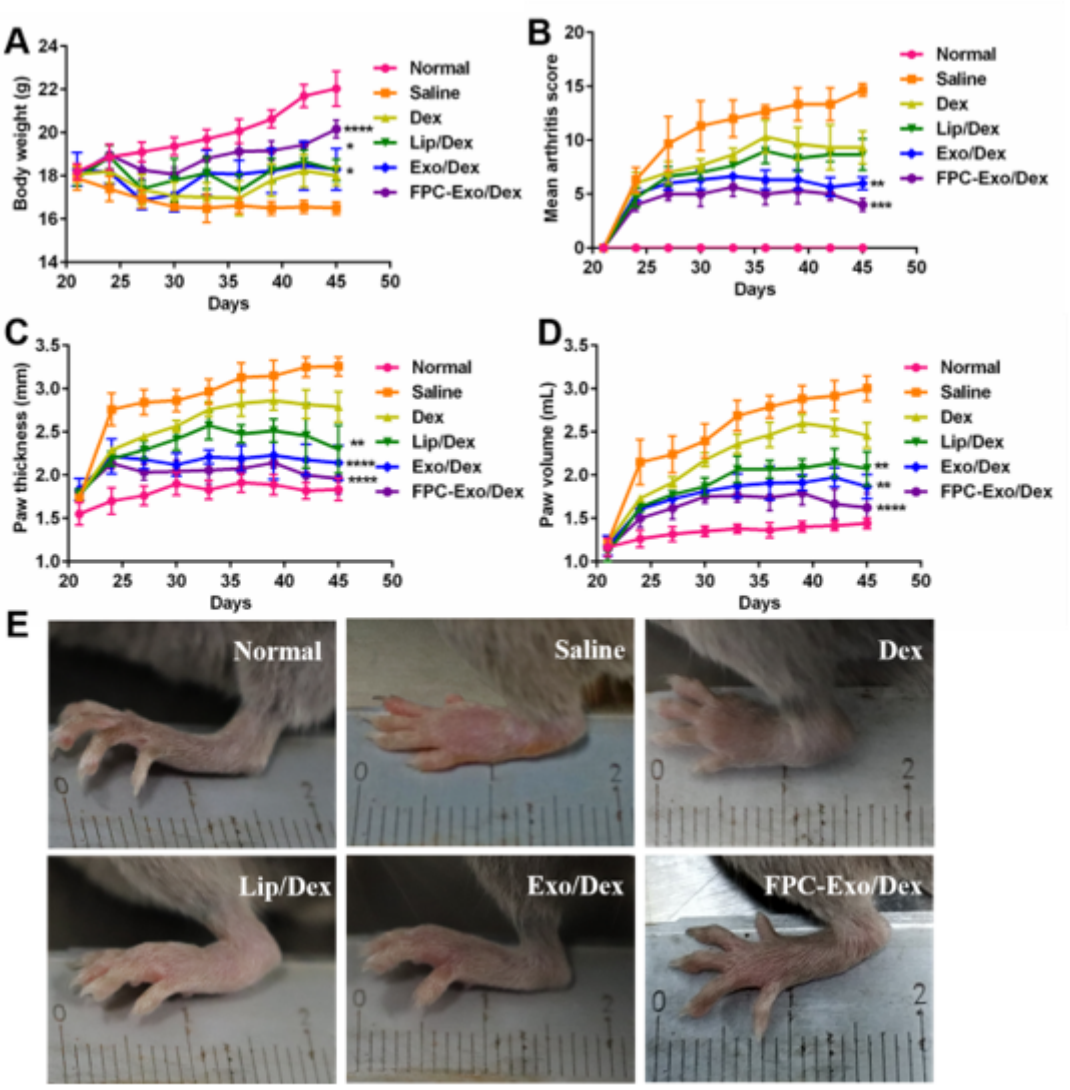

Figure 7

Therapeutic indicators monitoring during treatment. Measurement of body weight (A), articular score (B), paw thickness(C), paw volume (D) and photographs of representative hind limbs from animals treated with various Dex formulations in CIA mice (E). (n = 3, *p < 0.05, **p < 0.01, ***p < 0.001, ****p < 0.0001 vs mice injectedted with Saline).

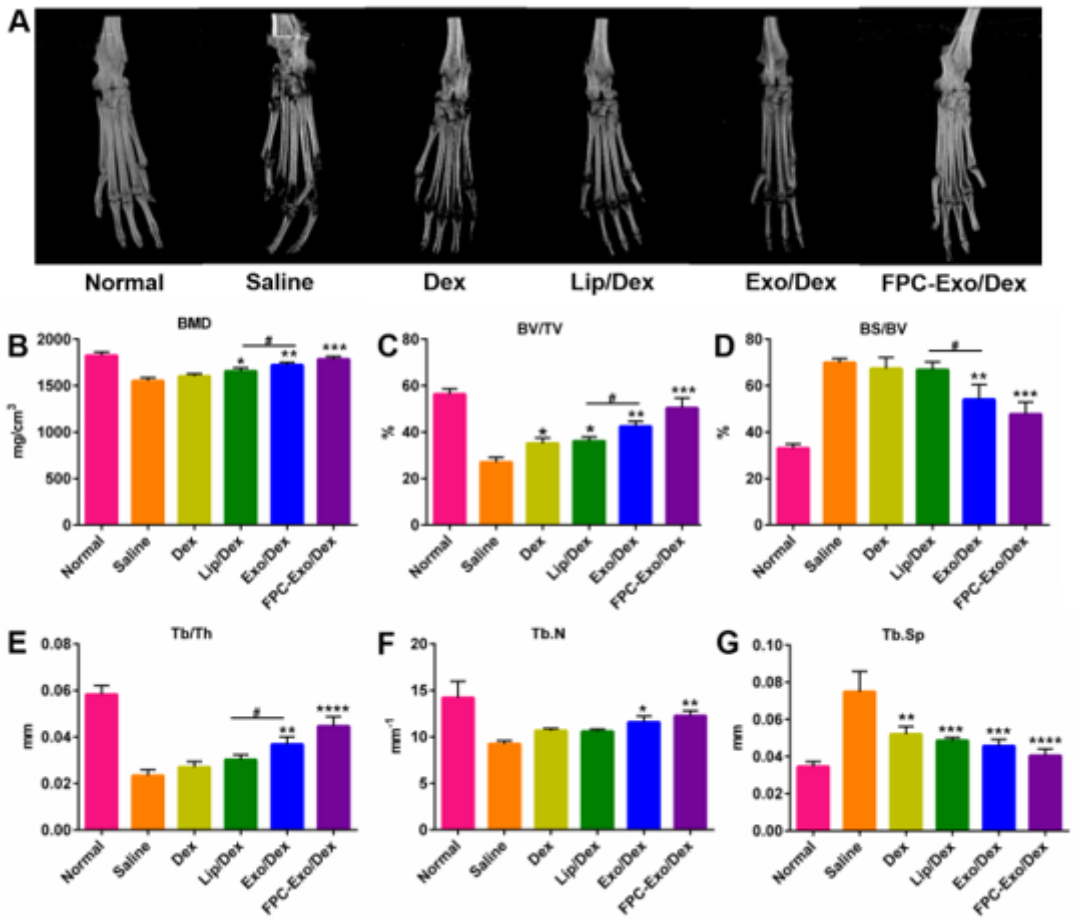

Figure 8

Micro-CT analyses of the hind limbs of the mice from different treatment groups. (A) Representative 3D reconstructed images from each treatment group. (B–G) Bone morphometric parameters of ROI within calcaneus bone (n = 3, *p < 0.05, **p < 0.01, ***p < 0.001, ****p < 0.0001 vs mice treated with Saline, #p < 0.05 is mice treated with Lip/Dex compared to Exo/Dex).

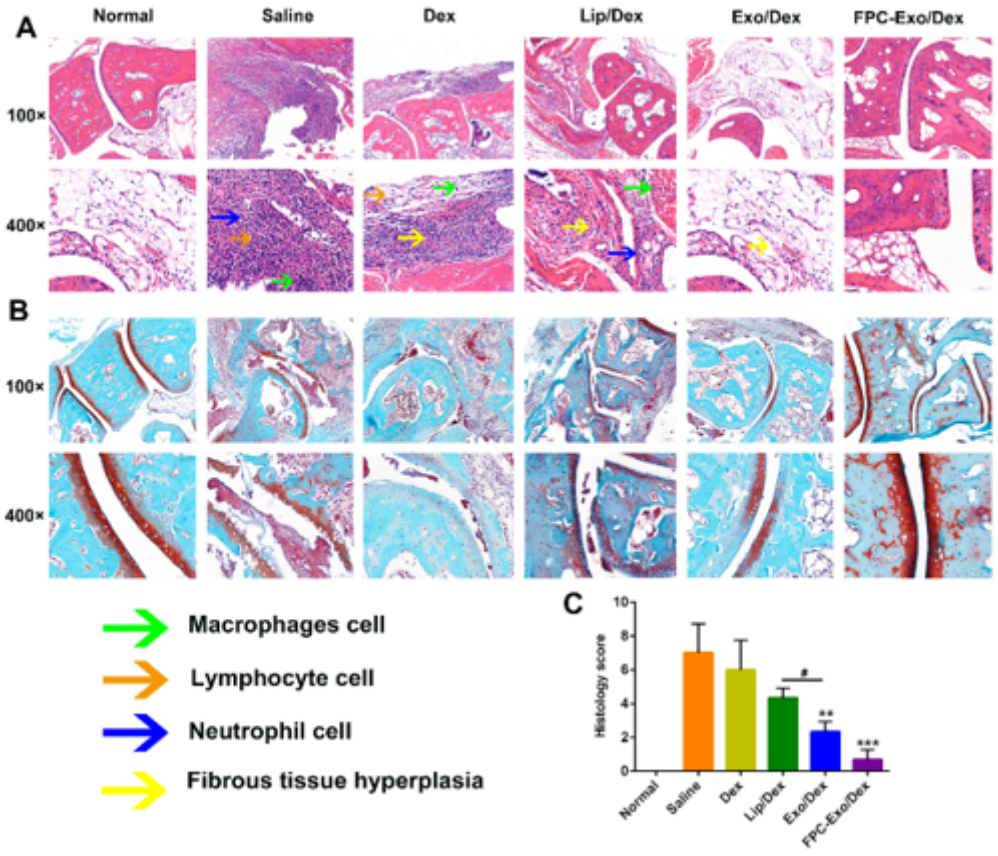

Figure 9

Histopathology analysis of the ankle joints. (A) Representative histopathology pictures of H&E staining. (B) Representative histopathology pictures of SO staining. (C) Histopathology scores of H&E staining (n = 3, **p < 0.01, ***p < 0.001 vs mice treated with Saline, #p < 0.05 is mice treated with Lip/Dex compared to with Exo/Dex).

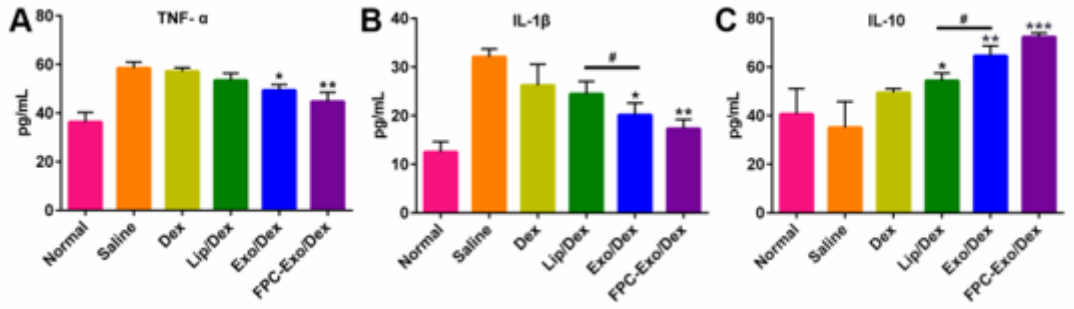

Figure 10

Levels of the inflammatory cytokines in serum. Level of TNF-α (A), IL-1β (B), and IL-10 (C), results are shown as mean ± SD (n = 3, *p < 0.05, **p < 0.01, ***p < 0.001 vs mice treated with Saline, #p < 0.05 is mice treated with Lip/Dex compared to Exo/Dex).

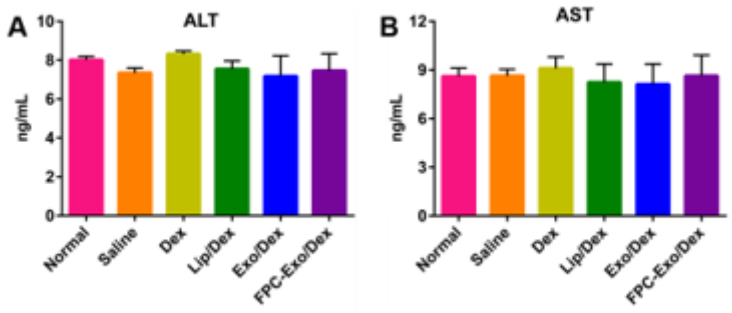

Figure 11

Levels of AST and ALT in serum (n = 3). All the treatment groups were compared to Normal group.

Supplementary Files

This is a list of supplementary files associated with this preprint. Click to download.

- supplement5.docx